Different Mechanisms of Alkaline and Enzymatic Hydrolysis of the Insensitive Munition Component 2,4-Dinitroanisole Lead to Identical Products

Bridget A. Ulrich,[†] Mallory Palatucci,[‡] Jakov Bolotin,[†] Jim C. Spain,[‡] and Thomas B. Hofstetter[*,†,¶]

Eawag, Swiss Federal Institute of Aquatic Science and Technology, CH-8600 Dübendorf, Switzerland, Center for Environmental Diagnostics & Bioremediation, University of West Florida, Pensacola, FL 32514-5751, USA, and Institute of Biogeochemistry and Pollutant Dynamics, ETH Zürich, CH-8092 Zürich, Switzerland

E-mail: thomas.hofstetter@eawag.ch

This document is the accepted manuscript version of the following article:
Ulrich, B. A., Palatucci, M., Bolotin, J., Spain, J. C., & Hofstetter, T. B. (2018). Different mechanisms of alkaline and enzymatic hydrolysis of the insensitive munition component 2,4-dinitroanisole lead to identical products. Environmental Science and Technology Letters, 5(7), 456-461. https://doi.org/10.1021/acs.estlett.8b00258

[*]To whom correspondence should be addressed
[†]Eawag
[‡]University of West Florida
[¶]ETH Zürich
This article was published online June 6, 2018: http://dx.doi.org/10.1021/acs.estlett.8b00258

Abstract

The emerging use of 2,4-dinitroanisole (DNAN) in insensitive munitions formulations has caused concern for future contamination of subsurface environments, generating significant interest in understanding and identifying its transformation processes. Here we characterized the C and N isotope fractionation associated with abiotic and biological DNAN hydrolysis through alkaline hydrolysis at high pH as well as enzymatic hydrolysis by *Nocardioides* sp. JS1661 and partially purified DNAN *O*-demethylase. Whereas both reactions generated 2,4-dinitrophenol (DNP), compound-specific isotope analysis (CSIA) of DNAN and DNP revealed that these reactions occur by different mechanisms. Alkaline hydrolysis was associated with apparent ^{13}C and ^{15}N kinetic isotope effects, ^{13}C-AKIE and ^{15}N-AKIE, of 1.044 ± 0.003 and 1.0027 ± 0.0004, respectively, reflecting the previously postulated nucleophilic aromatic substitution mechanism. Conversely, enzyme-catalyzed DNAN hydrolysis exhibited a ^{13}C-AKIE of 1.027 ± 0.005 and a ^{15}N-AKIE of 1.0032 ± 0.0003. Based on these AKIE values and the C and N isotope fractionation of DNP, our results imply that enzymatic *O*-demethylation of DNAN occurs through a nucleophilic substitution reaction at the aliphatic C of the methoxy group. This work provides a basis for the assessment of DNAN transformation by CSIA as the C and N isotope fractionation patterns observed in this work are distinct from other hypothesized degradation pathways.

Introduction

Soil and groundwater contamination due to the manufacture, use, and disposal of munitions compounds is a decades-old problem that continues to pose significant ecological and health risks.[1–4] As new formulations for insensitive munitions have emerged to replace conventional munitions, concern for future contamination has sparked interest in the environmental degradation pathways for these new energetic compounds. The nitroaromatic compound (NAC) 2,4-dinitroanisole (DNAN), developed as an alternative to 2,4,6-trinitrotoluene (TNT), is of particular interest due to its potential toxicity.[5,6] Similar to other NACs,[3,7–10] DNAN can be reduced to the corresponding aromatic amines[11–14] and transformed photolytically.[15–17] Interestingly, DNAN can also be hydrolyzed either abiotically at high pH[18,19] or biologically by DNAN *O*-demethylase from *Nocardioides* sp. JS1661 both of which form the same product, 2,4-dinitrophenol (DNP).[20,21] Therefore, assessing the extent and predominant routes of DNAN degradation will be challenging because the initial products are not only identical, but also transient.[15,22,23]

Compound-specific stable isotope analysis (CSIA) offers a strategy to distinguish between degradation processes without explicit need to monitor the concentration dynamics, and therefore may be especially useful for assessing DNAN degradation. Indeed, CSIA has proven useful for assessing both the pathways and extents of NAC degradation in contaminated soil.[24,25] This technique enables one to distinguish among degradation processes of NACs based on characteristic changes in $^{13}C/^{12}C$, $^{15}N/^{14}N$, and $^{2}H/^{1}H$ ratios that arise from kinetic isotope effects (KIE) at the reacting bond(s). Observations of this so-called isotope fractionation have also been applied to derive apparent KIEs as a means of elucidating NAC transformation mechanisms and kinetics.[26–34] CSIA could therefore be useful for identifying possible differences between abiotic and biological DNAN hydrolysis mechanisms.

Previous studies have suggested that alkaline hydrolysis of DNAN at high pH is initiated by nucleophilic aromatic substitution via a Meisenheimer intermediate (Scheme 1a).[18,19] However, little is known about the mechanism for enzymatic hydrolysis of DNAN by the DNAN *O*-demethylase.[20] Interestingly, the structurally similar herbicide dicamba (3,6-dichloro-2-methoxybenzoic acid) also

undergoes enzymatic *O*-demethylation, but this reaction is initated through oxidative substitution at the aliphatic C of the methoxy group.[35] Further, previously reported enzymatic *O*-demethylation reactions require O_2 or cofactors,[35,36] in contrast to enzymatic DNAN hydrolysis.[20] Therefore, the enzymatic hydrolysis of DNAN could potentially occur at the aliphatic C atom of the methoxy group. However, information for testing this mechanistic hypothesis is currently lacking.

The goal of this work was to delineate abiotic and biological DNAN hydrolysis reactions by CSIA, thus providing information for a stable-isotope based assessment of DNAN degradation in contaminated environments. We hypothesize that different mechanisms of alkaline and enzymatic hydrolysis will produce distinct isotope fractionation patterns despite the formation of identical transformation products. Moreover, the isotope fractionation associated with DNAN hydrolysis might differ from that expected for reduction as based on results from previous studies on other NACs. To this end, we characterized the C and N isotope fractionation from alkaline and enzymatic hydrolysis for both DNAN and the produced DNP, and derived the corresponding isotope enrichment factors (ϵ_C and ϵ_N) and apparent kinetic isotope effects (^{13}C-AKIE and ^{15}N-AKIE). Experiments were carried out in laboratory batch reactors containing homogeneous solutions at high pH,[19] the DNAN-degrading bacteria *Nocardioides* sp. JS1661, and partially purified DNAN *O*-demethylase.[20] Based on the correlations between C and N isotope fractionation of DNAN observed in the current work and previous studies with nitroaromatic contaminants,[29,31–33] we distinguish among the three most likely DNAN subsurface degradation processes by CSIA.

Materials and Methods

Alkaline and Enzymatic Hydrolysis Experiments

The procedure for the alkaline hydrolysis reactions was adapted from a method by Salter-Blanc et al.[19] Briefly, reactions were initiated upon introduction of 200 μL of a DNAN stock solution (50.5 mM in acetonitrile) into amber glass vials containing 20 mL of 50 mM phosphate buffer at pH 12, and were carried out at room temperature. Reactions were quenched at appropriate intervals

by adjusting the pH to 7.0 with 2 mL of dilute sulfuric acid. Samples of quenched reactions were analyzed by high performance liquid chromatography (HPLC) with UV-vis detection to quantify DNAN and DNP (Supplementary Information, SI, Section S1.1). Selected alkaline hydrolysis samples were also analyzed by liquid chromatography high resolution mass spectrometry (LC-HRMS) following methods described in Section S1.2 to confirm transformation product identity.

DNAN degradation by intact cells of *Nocardioides* sp. strain JS1661 cells was conducted in 1/4 strength Stanier's minimal medium[37] (pH 7.0, 25°C) and DNAN degradation by the partially purified enzyme preparation was conducted in HEPES buffer (0.02 M, pH 7.5), both of which initially contained 300 μM DNAN. Samples were removed from the incubation mixture at appropriate intervals, acidified to stop the reaction, filtered to 0.2 μm, and stored at 5°C until analyzed by HPLC (SI Section S1.2). Procedures for the growth of *Nocardioides* sp. strain JS1661 cells and the partial purification of DNAN *O*-demethylase were adapted from Karthikeyan and Spain[21] (Section S2). Though the DNAN starting material was obtained from the same source for both the alkaline and enzymatic hydrolysis experiments (Alfa Aesar, 98%), elemental analysis-IRMS revealed that the two batches of DNAN had different initial C and N isotope signatures (SI Section S3.1).

Isotopic Analyses

Isotopic analyses were conducted according to established procedures for gas chromatography isotope ratio mass spectrometry (GC-IRMS, details in Section S3).[38–40] Briefly, for analysis of $^{13}C/^{12}C$ and $^{15}N/^{14}N$ ratios of DNAN and DNP, the analytes were extracted by solid phase microextraction (SPME) after adjusting the solution pH to 7.2 (DNAN) or pH 2.1 (DNP). To derive C or N isotope enrichment factors (ϵ_C and ϵ_N) for each reaction, eqs. 1 and 2 below were fit to the measured $^{13}C/^{12}C$ and $^{15}N/^{14}N$ ratios.

$$\frac{\delta^h \mathrm{E}_{\mathrm{DNAN}} + 1}{\delta^h \mathrm{E}_{\mathrm{DNAN},0} + 1} = \left(\frac{c}{c_0}\right)^{\epsilon_\mathrm{E}} \tag{1}$$

$$\frac{\delta^h \mathrm{E_{DNP}} + 1}{\delta^h \mathrm{E_{DNAN,0}} + 1} = \frac{1 - (c/c_0)^{(\epsilon_\mathrm{E}+1)}}{1 - (c/c_0)} \tag{2}$$

where c/c_0 is the fraction of the remaining DNAN, ϵ_E is the C or N isotope enrichment factor, and $\delta^h \mathrm{E_{DNAN}}$ and $\delta^h \mathrm{E_{DNP}}$ are C and N isotope signature of DNAN and DNP (δ^{13}C or δ^{15}N). Procedures for the derivation of apparent ^{13}C and ^{15}N kinetic isotope effects (^{13}C- and ^{15}N-AKIEs) as well as the correlation of C and N isotope fractionation ($\Lambda^{\mathrm{N/C}}$) are provided in Section S4.2.

Results and Discussion

Alkaline Hydrolysis

Transformation of DNAN by alkaline hydrolysis at pH 12 followed pseudo-first order kinetics and concomittantly produced DNP as the only reaction product (Figure S4). DNAN and DNP concentrations accounted for 98% of the mass balance after 14 days. This interpretation is supported by an accurate description of the concentration dynamics with the stoichiometric transformation of DNAN to DNP with a single bimolecular hydrolysis rate constant, $k_{\mathrm{OH^-}}$, of $(2.5 \pm 0.2) \cdot 10^{-4}$ $\mathrm{M^{-1}s^{-1}}$ (Section S4.1 and Figure S4). Even though this number is determined only at pH 12, it is within the same order of magnitude as data from Salter-Blanc et al.[19] ($(7.1 \pm 0.5) \cdot 10^{-4}$ $\mathrm{M^{-1}s^{-1}}$), who determined $k_{\mathrm{OH^-}}$ more exhaustively over a wider range of pH values. DNP was identified through comparison of UV-vis spectra (Figure S1) and by its exact mass by LC-HRMS (Figures S2a-c). We found no evidence for a stable Meisenheimer intermediate postulated by others[18,19] (Section S1.2).

Alkaline hydrolysis of DNAN was associated with considerable C and N isotope fractionation (Figure 1a/b) corresponding to isotope enrichment factors, ϵ_C and ϵ_N, of -6.0 ± 0.5‰ and -2.7 ± 0.4‰, respectively (Table 1). Based on previous evidence[18,19] and the stoichiometric formation of DNP observed here, we derived apparent ^{13}C and ^{15}N kinetic isotope effects (AKIEs) of 1.044 ± 0.003 and 1.0027 ± 0.0004, respectively, assuming transformation of DNAN through

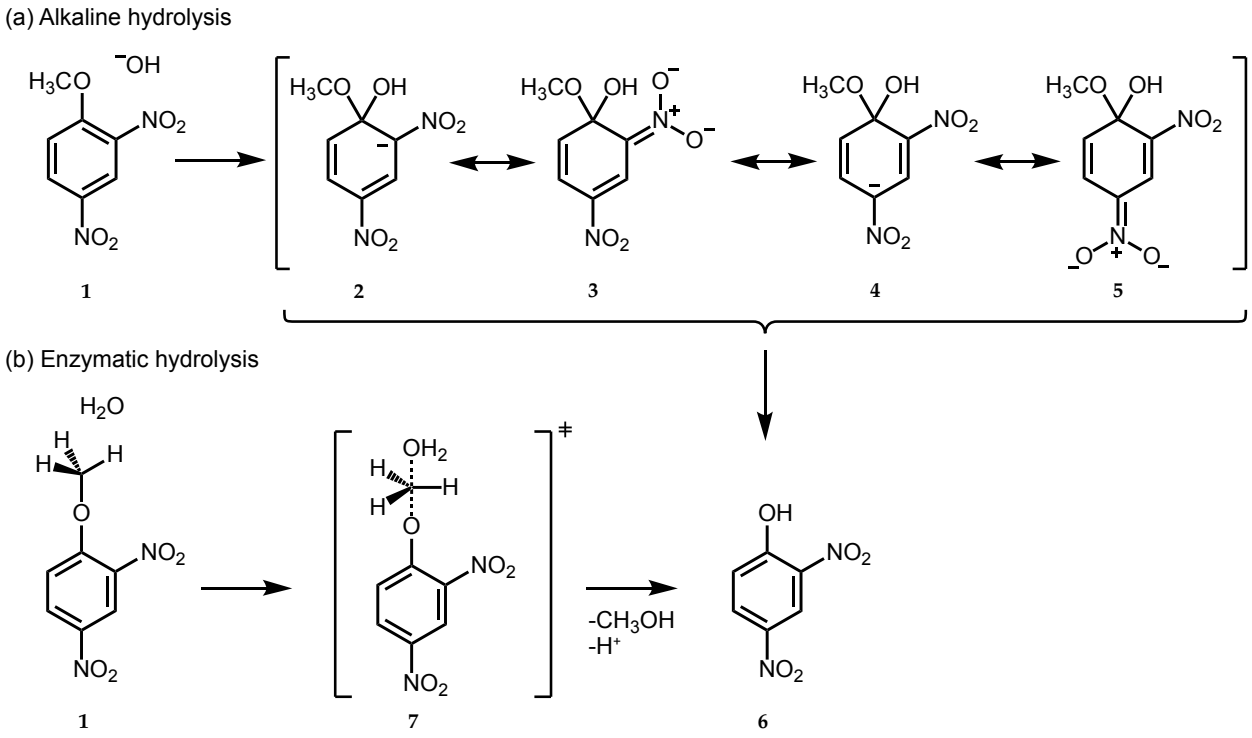

Scheme 1 Initial steps for the transformation of 2,4-dinitroanisole (**1**) by (a) alkaline hydrolysis through nucleophilic aromatic substitution to 2,4-dinitrophenol (**6**). Compounds **2** to **5** are resonance structures of the Meisenheimer complex intermediates.[18] (b) Hypothesized enzymatic hydrolysis of DNAN by *Nocardioides* sp. JS1661 and enzyme assays containing DNAN *O*-demethylase. Compound **7** shows one of several possible transition states for a hydrolytic *O*-demethylation at the aliphatic C atom of the methoxy group.

nucleophilic aromatic substitution (Scheme 1a). Although there is no precedent for ^{13}C and ^{15}N isotope effects from such reactions, it is plausible that the substantial bonding changes at the aromatic C atoms cause large ^{13}C AKIEs, whereas the ^{15}N AKIE reflects a secondary effect for N atoms not directly involved in the nucleophilic attack. A comparison with the similarly large ^{13}C-AKIE of 1.047 ± 0.002 for the alkaline hydrolysis of atrazine at pH 12 supports this interpretation.[41,42]

The $\delta^{13}C$ of DNP increases substantially with reaction progress. The ϵ_C of -8.9 ± 1.4‰ calculated from eq. 2 with $\delta^{13}C$ of DNP exceeds that derived from data for DNAN because C isotope fractionation in DNP is not diluted by the non-reactive C in the methoxy group ($-OCH_3$). This observation is consistent with a reaction mechanism in which only aromatic C atoms are affected by nucleophilic attack (Scheme 1a). However, contrary to expectations from the large

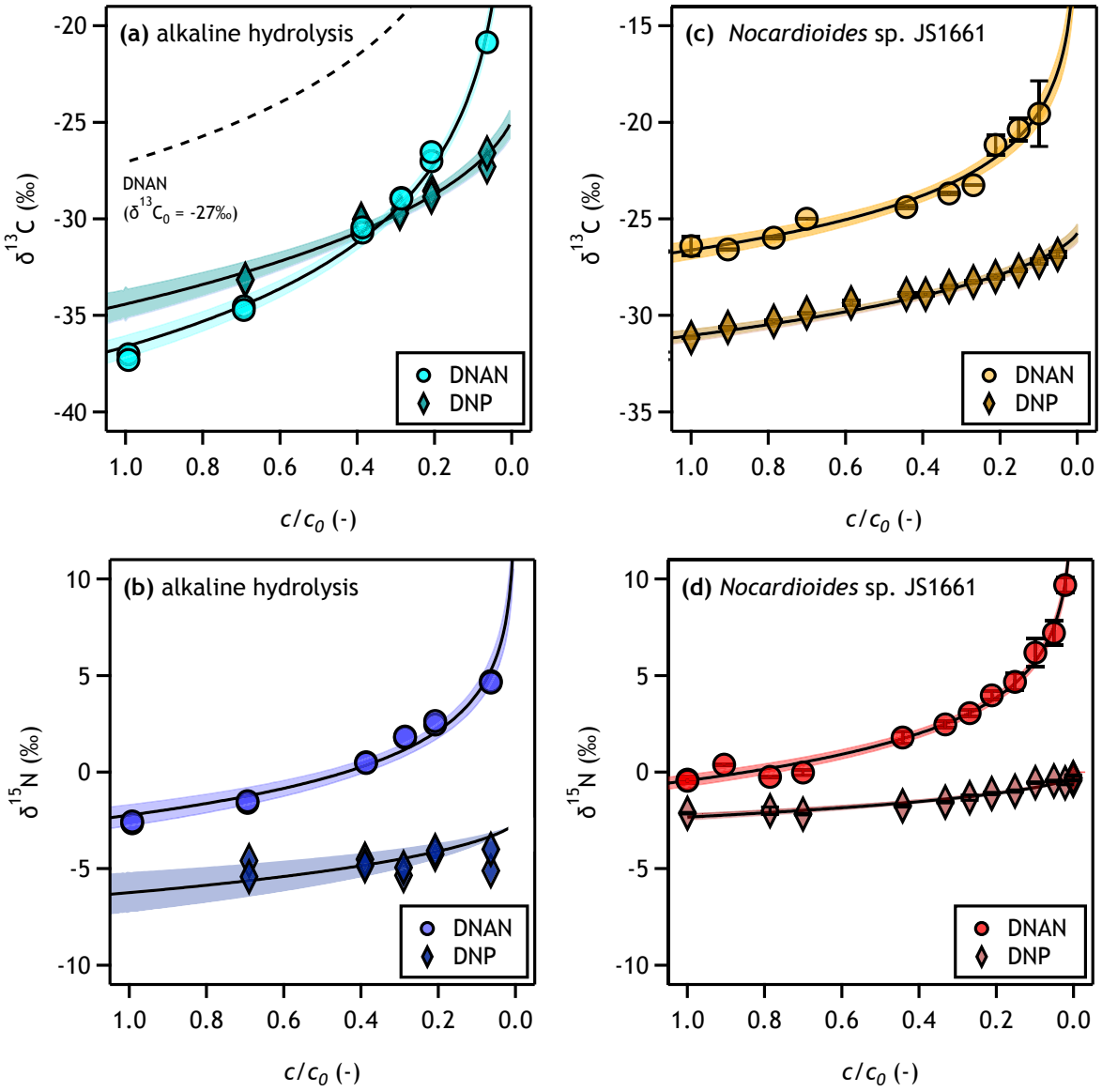

Figure 1 C and N isotope fractionation associated with the transformation of DNAN to DNP by alkaline hydrolysis at pH 12 (panels a and b) and during biodegradation by *Nocardioides* sp. JS1661 (panels c and d). Panels (a) and (b) show δ^{13}C of DNAN and DNP vs. fraction of remaining DNAN, c/c_0; panels (c) and (d) show the corresponding δ^{15}N trends. Lines represent non-linear fits of eqs. 1 and 2) for DNAN and DNP, respectively (data in Tables 1 and S2). The dashed line in panel (a) represents the hypothetical case for DNAN where there is homogeneous intramolecular δ^{13}C distribution among aromatic and aliphatic C atoms of $-27‰$. Shaded areas indicate the 95% confidence intervals.

normal ^{13}C-AKIE, which implies a preferential transformation of ^{12}C isotopologues of DNAN, DNP is not enriched in ^{12}C compared to DNAN. In fact, even after 30% of DNAN conversion (i.e., $c/c_0 = 0.7$, Figure 1a) the δ^{13}C of DNP is larger than that of DNAN, meaning that the produced DNP contains more ^{13}C than DNAN. This positive shift of δ^{13}C value of DNP reflects an uneven intramolecular ^{13}C/^{12}C distribution of aromatic and aliphatic C atoms in the DNAN starting material. The non-reactive aromatic C atoms of DNAN exhibit a δ^{13}C of between −25‰ to −27‰ as derived from fitting eq. 2 to δ^{13}C of DNP and from the final δ^{13}C of DNP after 95% DNAN conversion. A mass balance calculation (Section S4.3) reveals that the C atom of the OCH_3 group was isotopically very light (−99‰ to −110‰) and substantially more negative than existing data for this functional group in organic compounds.[43]

While the magnitude of C isotope fractionation due to alkaline hydrolysis of DNAN to DNP quantified with eqs. 1 and 2 is independent of the intramolecular C isotope distribution in DNAN, the position of the isotope fractionation trajectories on the y-axis in Figure 1a may shift considerably (Figure 1a). As a comparison, Figure 1a also illustrates the behavior expected for isotopically homogenous DNAN. If the δ^{13}C of the OCH_3 group would correspond to that of the aromatic C atoms (e.g., −27‰), the DNAN fractionation curve would be shifted upwards in Figure 1a (dashed line). At low stages of conversion, i.e., $c/c_0 > 0.9$, the offset of the DNAN and DNP C isotope fractionation curve would be identical to the ϵ_C value for alkaline hydrolysis of −6.0‰ (eq. S7).

The ϵ_N for alkaline hydrolysis determined from DNAN and DNP with eqs. 1 and 2 agree within uncertainty (-2.7 ± 0.4‰ and -3.6 ± 1.0‰, Tables 1 and S2). Contrary to the above observations, N isotope fractionation was not affected by intramolecular isotope distribution because DNAN and DNP contain all N atoms in the non-reactive NO_2 substituents. However, the δ^{15}N for DNP at 95% substrate conversion was still slightly lower than that for the unreacted substrate (-4.6 ± 1.0‰ versus -2.6 ± 0.2‰, respectively), which was likely due to a combination of analytical error and the reaction not quite reaching completion.

Table 1 Carbon and and nitrogen isotope enrichment factors (ϵ_C, ϵ_N), apparent ^{13}C and ^{15}N kinetic isotope effects (^{13}C-AKIE, ^{15}N-AKIE), and correlation of C and N isotope fractionation ($\Lambda^{N/C}$) associated with the alkaline and enzymatic hydrolysis of DNAN.[a,b]

System	ϵ_C (‰)	ϵ_N (‰)	^{13}**C-AKIE** (-)	^{15}**N-AKIE** (-)	$\Lambda^{N/C}$ (-)
Alkaline hydrolysis	−6.0 ± 0.5	−2.7 ± 0.4	1.044 ± 0.003	1.0027 ± 0.0004	0.46 ± 0.04
Nocardioides sp. JS1661					
Whole cell experiments	−2.8 ± 0.1	−2.5 ± 0.1	1.020 ± 0.003	1.0025 ± 0.0001	0.87 ± 0.15
Partially purified enzyme	−3.7 ± 0.1	−3.2 ± 0.1	1.027 ± 0.005	1.0032 ± 0.0003	1.06 ± 0.25

[a] Combination of replicate experiments according to methods of Scott et al.[44], assumptions for calculations with eq. S6. ^{13}C-AKIE: $n_C = 7$, $x = z = 1$; ^{15}N-AKIE: $n = x = z = 1$ according to the assumption of a secondary isotope effect, see Section S4.2; [b] Slope of a linear regression analysis of $\delta^{15}N$ vs. $\delta^{13}C$, uncertainties denote 95% confidence intervals.

Enzymatic Hydrolysis

Transformation of DNAN by *Nocardioides* sp. JS1661 led to the stoichiometric formation of DNP after 80 minutes (Figure S3a), in agreement with previous work.[20] Compared to alkaline hydrolysis, the disappearance of DNAN was associated with smaller C isotope fractionation and similar N isotope fractionation (Figure 1c/d), with ϵ_C and ϵ_N values of -2.8 ± 0.1‰ and -2.5 ± 0.1‰, respectively. Experiments with partially purified *O*-demethylase (Figure S3b) revealed DNAN C and N isotope fractionation that was approximately 30% stronger than for whole cell experiments (Figure S5). ϵ_C and ϵ_N were -3.7 ± 0.1‰ and -3.2 ± 0.1‰, respectively (Table 1). The correlations between C and N isotope fractionation, which are indicative of the reaction mechanisms, resulted in identical slopes, $\Lambda^{N/C}$, within experimental uncertainty (0.87 ± 0.15 vs. 1.06 ± 0.25, respectively, Table 1 and Figure S6). Moreover, $\Lambda^{N/C}$ also corresponded well with the ratio ϵ_N/ϵ_C (0.86 ± 0.04 and 0.89 ± 0.05, respectively). Therefore, the differences between the experiments with whole cells and partially purified enzyme were presumably caused by the masking of isotope fractionation through mass transfer limitations associated with substrate uptake.[45]

Based on the assumption that there is one reactive position for nucleophilic attack, we obtained ^{13}C and ^{15}N-AKIEs of 1.027 ± 0.005 and 1.0032 ± 0.0003, respectively, for enzyme-catalyzed DNAN hydrolysis (Table 1). Whereas the ^{15}N-AKIEs of alkaline and enzymatic DNAN are identical and consistent with reactions that do not involve the aromatic NO_2 groups, the ^{13}C-AKIEs differ considerably. These differences also result in distinct $\Lambda^{N/C}$-values (Table 1) and imply that enzymatic DNAN hydrolysis occurs by a mechanism that is different from that for alkaline hydrolysis. The isotope effects reported here for DNAN hydrolysis by DNAN *O*-demethylase are consistent with a nucleophilic substitution reaction at the aliphatic C of the OCH_3 group (Scheme 1b, **1** → **6**). This interpretation is supported by known ^{13}C AKIEs for nucleophilic substitutions at aliphatic C atoms in C–O bonds, for example, a ^{13}C-AKIE of 1.025 for methyl tert-butyl ether hydrolysis.[46] Further, bimolecular nucleophilic substitutions through formation of a tetrahedral intermediate such as **7** in Scheme 1 also exhibit very moderate secondary H isotope fractionation, which is consistent with our evaluation of H isotope fractionation for the enzyme-catalyzed hydrolysis of DNAN (Figure S7). Moreover, secondary ^{15}N-AKIEs ≤ 1.005 agree with evidence from the attack of nucleophilic oxygen at several types of acyl groups, including carboxylic esters and amides, through formation of tetrahedral intermediates.[47–49]

This mechanism for enzymatic DNAN hydrolysis at the aliphatic C of the OCH_3 group is further supported by the C isotope fractionation observed in the reaction product DNP (Figure 1c). Whereas the magnitude of N isotope fractionation of DNP is consistent with that of DNAN in both enzymatic and alkaline hydrolysis experiment (Table S2), the δ^{13}C trends of DNP from enzymatic and alkaline hydrolysis (Figures 1c and 1a, respectively) are quite different. In particular, enrichment of ^{13}C in DNP during its formation from enzymatic hydrolysis spans a smaller range of δ^{13}C values than for DNP formed during alkaline hydrolysis (see ϵ_C-values in Table S2). This moderate C isotope fractionation in DNP is consistent with the above assumption that DNP formed enzymatically originates from a reaction that, in contrast to alkaline hydrolysis, did not involve aromatic C atoms.

Environmental Implications

Because alkaline and enzymatic hydrolysis of DNAN showed differences in C isotope fractionation but not in N isotope fractionation, the correlation of C and N isotope fractionation results in distinct trendlines (Figure 2, $\Lambda^{N/C}$ of 0.46 ± 0.04 vs. 0.87 ± 0.15 for alkaline and enzymatic hydrolysis, respectively). These trends are also different from previously reported isotope fractionation for biological or abiotic reductions of structurally similar NACs exhibiting large $\Lambda^{N/C}$ (green trajectories in Figure 2).[25,29,33,50] These results not only imply that the abiotic and biological hydrolysis of DNAN occur by different mechanisms, but also that these processes can be discerned from other potential degradation pathways based on C and N fractionation of DNAN. Moreover, this work could potentially provide a mechanistic precedent if *O*-demethylation reactions are identified from other organic contaminants.

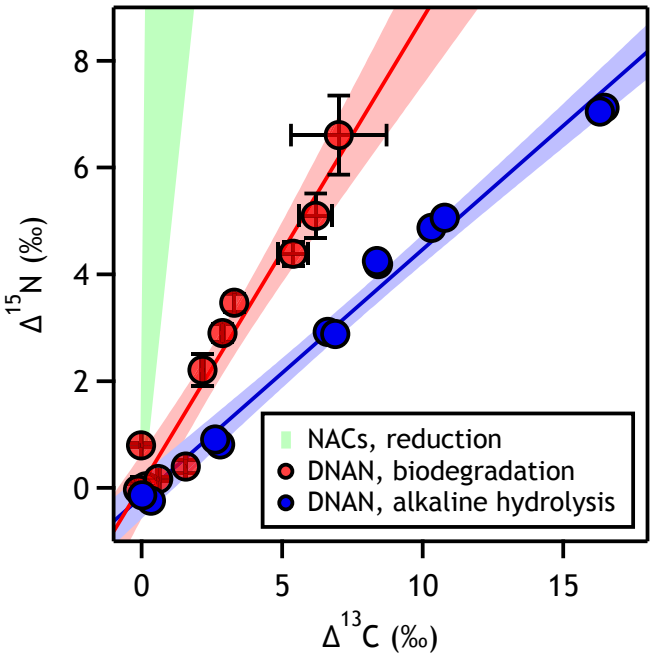

Figure 2 Correlation of C and N isotope fractionation for the alkaline and enzymatic hydrolysis of DNAN compared to expected trends for DNAN reduction (according to trends previously observed for the biotic and abiotic reduction of other NACs).[25,29,33,50] Solid lines and shaded areas denote linear regressions and 95% confidence intervals, respectively, for alkaline and enzymatic hydrolysis ($\Lambda^{N/C}_{\text{biodegradation}} = 0.87 \pm 0.15$, $\Lambda^{N/C}_{\text{alkaline hydrolysis}} = 0.46 \pm 0.04$). The expected range for DNAN reduction is shaded in green ($\Lambda^{N/C}_{\text{reduction}} \approx 5 - 50$).

Acknowledgement

Bridget Ulrich was supported by the Strategic Environmental Research and Development Program (SERDP Project no. ER-2618).

Supporting Information Available

Details relating to chemical analyses, cell growth and enzyme partial purification, stable isotope analysis, data evaluation, reaction kinetics, and additional isotope fractionation data. This material is available free of charge via the Internet at `http://pubs.acs.org/`.

References

(1) Rodgers, J. D.; Bunce, N. J. Treatment methods for the remediation of nitroaromatic explosives. *Water Res.* **2001**, *35*, 2101–2111.

(2) Ryu, H.; Han, J. K.; Jung, J. W.; Bae, B.; Nam, K. Human health risk assessment of explosives and heavy metals at a military gunnery range. *Environ. Geochem. Health* **2007**, *29*, 259–269.

(3) Spain, J. C.; Hughes, J. B.; Knackmuss, H.-J. *Biodegradation of Nitroaromatic Compounds and Explosives*; Lewis Publishers, Boca Raton, 2000; p 434.

(4) Sunahara, G. I., Lotufo, G. R., Sunahara, G., Kuperman, R. G., Kuperman, R., Hawari, J., Eds. *Ecotoxicology of Explosives*; CRC Press, 2009.

(5) Dodard, S. G.; Sarrazin, M.; Hawari, J.; Paquet, L.; Ampleman, G.; Thiboutot, S.; Sunahara, G. I. Ecotoxicological assessment of a high energetic and insensitive munitions compound: 2,4-dinitroanisole (DNAN). *J. Hazard. Mater.* **2013**, *262*, 143–150.

(6) Liang, J.; Olivares, C. I.; Field, J. A.; Sierra-Alvarez, R. Microbial toxicity of the insensitive munitions compound, 2,4-dinitroanisole (DNAN), and its aromatic amine metabolites. *J. Hazard. Mater.* **2013**, *262*, 281–287.

(7) Hofstetter, T. B.; Heijman, C. G.; Haderlein, S. B.; Holliger, C.; Schwarzenbach, R. P. Complete reduction of TNT and other (poly)nitroaromatic compounds under iron reducing subsurface conditions. *Environ. Sci. Technol.* **1999**, *33*, 1479–1487.

(8) Ju, K. S.; Parales, R. E. Nitroaromatic compounds, from synthesis to biodegradation. *Microbiol. Mol. Biol. Rev.* **2010**, *74*, 250–272.

(9) Emmrich, M. Kinetics of the alkaline hydrolysis of important nitroaromatic co-contaminants of 2,4,6-trinitrotoluene in highly contaminated soils. *Environ. Sci. Technol.* **2001**, *35*, 874–877.

(10) Luning Prak, D. J.; Breuer, J. E. T.; Rios, E. A.; Jedlicka, E. E.; O'Sullivan, D. W. Photolysis of 2,4,6-trinitrotoluene in seawater and estuary water: Impact of pH, temperature, salinity, and dissolved organic matter. *Mar. Pollut. Bull.* **2017**, *114*, 977–986.

(11) Olivares, C. I.; Liang, J.; Abrell, L.; Sierra-Alvarez, R.; Field, J. A. Pathways of reductive 2,4-dinitroanisole (DNAN) biotransformation in sludge. *Biotechnol. Bioeng.* **2013**, *110*, 1595–1604.

(12) Perreault, N. N.; Manno, D.; Halasz, A.; Thiboutot, S.; Ampleman, G.; Hawari, J. Aerobic biotransformation of 2,4-dinitroanisole in soil and soil *Bacillus* sp. *Biodegradation* **2012**, *23*, 287–295.

(13) Niedźwiecka, J. B.; Drew, S. R.; Schlautman, M. A.; Millerick, K. A.; Grubbs, E.; Tharayil, N.; Finneran, K. T. Iron and electron shuttle mediated (bio)degradation of 2,4-dinitroanisole (DNAN). *Environ. Sci. Technol.* **2017**, *51*, 10729–10735.

(14) Olivares, C. I.; Madeira, C. L.; Sierra-Alvarez, R.; Kadoya, W.; Abrell, L.; Chorover, J.; Field, J. A. Environmental fate of ^{14}C radiolabeled 2,4-dinitroanisole in soil microcosms. *Environ. Sci. Technol.* **2017**, *51*, 13327–13334.

(15) Hawari, J.; Monteil-Rivera, F.; Perreault, N. N.; Halasz, A.; Paquet, L.; Radovic-Hrapovic, Z.;

Deschamps, S.; Thiboutot, S.; Ampleman, G. Environmental fate of 2,4-dinitroanisole (DNAN) and its reduced products. *Chemosphere* **2015**, *119*, 16–23.

(16) Halasz, A.; Hawari, J.; Perreault, N. N. New insights into the photochemical degradation of theinsensitive munition formulation IMX-101 in Water. *Environ. Sci. Technol.* **2018**, *52*, 589–596.

(17) Schroer, H. W.; Li, X.; Lehmler, H.-J.; Just, C. L. Metabolism and photolysis of 2,4-dinitroanisole in arabidopsis. *Environ. Sci. Technol.* **2017**, *51*, 13714–13722.

(18) Sviatenko, L.; Kinney, C. A.; Gorb, L.; Hill, F. C.; Bednar, A. J.; Okovytyy, S.; Leszczynski, J. Comprehensive investigations of kinetics of alkaline hydrolysis of TNT (2,4,6-trinitrotoluene), DNT (2,4-dinitrotoluene), and DNAN (2,4-dinitroanisole). *Environ. Sci. Technol.* **2014**, *48*, 10465–10474.

(19) Salter-Blanc, A. J.; Bylaska, E. J.; Ritchie, J. J.; Tratnyek, P. G. Mechanisms and kinetics of alkaline hydrolysis of the energetic nitroaromatic compounds 2,4,6-trinitrotoluene (TNT) and 2,4-dinitroanisole (DNAN). *Environ. Sci. Technol.* **2013**, *47*, 6790–6798.

(20) Fida, T. T.; Palamuru, S.; Pandey, G. P.; Spain, J. C. Aerobic biodegradation of 2,4-dinitroanisole by *Nocardioides* sp strain JS1661. *Appl. Environ. Microbiol.* **2014**, *80*, 7725–7731.

(21) Karthikeyan, S.; Spain, J. C. Biodegradation of 2, 4-dinitroanisole (DNAN) by *Nocardioides* sp. JS1661 in water, soil and bioreactors. *J. Hazard. Mater.* **2016**, *312*, 37–44.

(22) Schroer, H. W.; Langenfeld, K. L.; Li, X.; Lehmler, H.-J.; Just, C. L. Stable isotope-enabled pathway elucidation of 2,4-dinitroanisole metabolized by *Rhizobium lichtii*. *Environ. Sci. Technol. Lett.* **2015**, *2*, 362–366.

(23) Richard, T.; Weidhaas, J. L. Biodegradation of IMX-101 explosive formulation constituents:

2,4-Dinitroanisole (DNAN), 3-nitro-1,2,4-triazol-5-one (NTO), and nitroguanidine. *J. Hazard. Mater.* **2014**, *280*, 372–379.

(24) Hofstetter, T. B.; Bolotin, J.; Pati, S. G.; Skarpeli-Liati, M.; Spahr, S.; Wijker, R. S. Isotope effects as new proxies for organic pollutant transformation. *CHIMIA* **2014**, *68*, 788–792.

(25) Wijker, R. S.; Bolotin, J.; Nishino, S. F.; Spain, J. C.; Hofstetter, T. B. Using compound-specific isotope analysis to assess biodegradation of nitroaromatic explosives in the subsurface. *Environ. Sci. Technol.* **2013**, *47*, 6872–6883.

(26) Pati, S. G.; Kohler, H.-P. E.; Bolotin, J.; Parales, R. E.; Hofstetter, T. B. Isotope Effects of enzymatic dioxygenation of nitrobenzene and 2-nitrotoluene by nitrobenzene dioxygenase. *Environ. Sci. Technol.* **2014**, *48*, 10750–10759.

(27) Pati, S. G.; Kohler, H.-P. E.; Pabis, A.; Paneth, P.; Parales, R. E.; Hofstetter, T. B. Substrate and enzyme specificity of the kinetic isotope effects associated with the dioxygenation of nitroaromatic contaminants. *Environ. Sci. Technol.* **2016**, *50*, 6708–6716.

(28) Wijker, R. S.; Pati, S. G.; Zeyer, J.; Hofstetter, T. B. Enzyme kinetics of different types of flavin-dependent monooxygenases determine the observable contaminant stable isotope fractionation. *Environ. Sci. Technol. Lett.* **2015**, *2*, 329–334.

(29) Wijker, R. S.; Zeyer, J.; Hofstetter, T. B. Isotope fractionation associated with the simultaneous biodegradation of multiple nitrophenol isomers by *Pseudomonas putida* B2. *Environ. Sci.-Process Impacts* **2017**, *74*, 775–784.

(30) Hartenbach, A.; Hofstetter, T. B.; Berg, M.; Bolotin, J.; Schwarzenbach, R. P. Using nitrogen isotope fractionation to assess abiotic reduction of nitroaromatic compounds. *Environ. Sci. Technol.* **2006**, *40*, 7710–7716.

(31) Hartenbach, A.; Hofstetter, T. B.; Aeschbacher, M.; Sander, M.; Kim, D.; Strathmann, T. J.; Arnold, W. A.; Cramer, C. J.; Schwarzenbach, R. P. Variability of nitrogen isotope fraction-

ation during the reduction of nitroaromatic compounds with dissolved reductants. *Environ. Sci. Technol.* **2008**, *42*, 8352–8359.

(32) Hofstetter, T. B.; Neumann, A.; Arnold, W. A.; Hartenbach, A. E.; Bolotin, J.; Cramer, C. J.; Schwarzenbach, R. P. Substituent effects on nitrogen isotope fractionation during abiotic reduction of nitroaromatic compounds. *Environ. Sci. Technol.* **2008**, *42*, 1997–2003.

(33) Hofstetter, T. B.; Spain, J. C.; Nishino, S. F.; Bolotin, J.; Schwarzenbach, R. P. Identifying competing aerobic nitrobenzene biodegradation pathways using compound-specific isotope analysis. *Environ. Sci. Technol.* **2008**, *42*, 4764–4770.

(34) Stewart, S. M.; Hofstetter, T. B.; Joshi, P. A.; Gorski, C. A. Linking thermodynamics to pollutant reduction kinetics by Fe^{2+} bound to iron oxides. *Environ. Sci. Technol.* **2018**, *52*, 5600–5609.

(35) Dumitru, R.; Jiang, W.; Weeks, D.; Wilson, M. Crystal structure of dicamba monooxygenase: A Rieske nonheme oxygenase that catalyzes oxidative demethylation. *J. Mol. Biol.* **2009**, *392*, 498–510.

(36) Yao, L.; Jia, X.; Zhao, J.; Cao, Q.; Xie, X.; Yu, L.; He, J.; Tao, Q. Degradation of the herbicide dicamba by two sphingomonads via different *O*-demethylation mechanisms. *International Biodeterioration and Biodegradation* **2015**, *104*, 324–332.

(37) Cohen-Bazire, G.; Sistrom, W. R.; Stanier, R. Y. Kinetic studies of pigment synthesis by non-sulfur purple bacteria. *J. Cell Physiol.* **1957**, *49*, 25–68.

(38) Pati, S. G.; Kohler, H.-P. E.; Hofstetter, T. B. In *Measurement and Analysis of Kinetic Isotope Effects*; Harris, M. E., Anderson, V. E., Eds.; Academic Press, 2017; pp 292–329.

(39) Berg, M.; Bolotin, J.; Hofstetter, T. B. Compound-specific nitrogen and carbon isotope analysis of nitroaromatic compounds in aqueous samples using solid-phase microextraction coupled to GC/IRMS. *Anal. Chem.* **2007**, *79*, 2386–2393.

(40) Spahr, S.; Huntscha, S.; Bolotin, J.; Meier, M. P.; Elsner, M.; Hollender, J.; Hofstetter, T. B. Compound-specific isotope analysis of benzotrizale and its derivatives. *Anal. Bioanal. Chem.* **2013**, *405*, 2843–2856.

(41) Meyer, A. H.; Penning, H.; Elsner, M. C and N isotope fractionation suggests similar mechanisms of microbial atrazine transformation despite involvement of different enzymes (AtzA and TrzN). *Environ. Sci. Technol.* **2009**, *43*, 8079–8085.

(42) Grzybkowska, A.; Kaminski, R.; Dybala-Defratyka, A. Theoretical predictions of isotope effects versus their experimental values for an example of uncatalyzed hydrolysis of atrazine. *Phys. Chem. Chem. Phys.* **2014**, *16*, 15164–15172.

(43) Hoehener, P.; Silvestre, V.; Lefrancois, A.; Loquet, D.; Botosoa, E. P.; Robins, R. J.; Remaud, G. S. Analytical model for site-specific isotope fractionation in ^{13}C during sorption: Determination by isotopic ^{13}C NMR spectrometry with vanillin as model compound. *Chemosphere* **2012**, *87*, 445–452.

(44) Scott, K. M.; Lu, X.; Cavanaugh, C. M.; Liu, J. S. Optimal methods for estimating kinetic isotope effects from different forms of the Rayleigh distillation equation. *Geochim. Cosmochim. Acta* **2004**, *68*, 433–442.

(45) Thullner, M.; Fischer, A.; Richnow, H.-H.; Wick, L. Y. Influence of mass transfer on stable isotope fractionation. *Appl. Microbiol. Biotechnol.* **2013**, *97*, 441–452.

(46) Elsner, M.; McKelvie, J.; Lacrampe-Couloume, G.; Sherwood Lollar, B. Insight into methyl *tert*-butyl ether (MTBE) stable isotope fractionation from abiotic reference experiments. *Environ. Sci. Technol.* **2007**, *41*, 5693–5700.

(47) Robins, L. I.; Fogle, E. J.; Marlier, J. F. Mechanistic investigations of the hydrolysis of amides, oxoesters and thioesters via kinetic isotope effects and positional isotope exchange. *Biochimica et Biophysica Acta (BBA) - Proteins and Proteomics* **2015**, *1854*, 1756–1767.

(48) Marlier, J. F.; Campbell, E.; Lai, C.; Weber, M.; Reinhardt, L. A.; Cleland, W. W. Multiple isotope effect study of the acid-catalyzed hydrolysis of formamide. *J. Org. Chem.* **2006**, *71*, 3829–3836.

(49) Marlier, J. F. Multiple isotope effects on the acyl group transfer reactions of amides and esters. *Acc. Chem. Res.* **2001**, *34*, 283–290.

(50) Wijker, R. S.; Kurt, Z.; Spain, J. C.; Bolotin, J.; Zeyer, J.; Hofstetter, T. B. Isotope fractionation associated with the biodegradation of 2- and 4-nitrophenols via monooxygenation pathways. *Environ. Sci. Technol.* **2013**, *47*, 14185–14193.

Graphical Abstract